

## Measurements of the Shear Alfvén Wave Dispersion for Finite Perpendicular Wave Number

C. A. Kletzing,\* S. R. Bounds, and J. Martin-Hiner

*Department of Physics and Astronomy, University of Iowa, 203 Van Allen Hall, Iowa City, Iowa 52245*

W. Gekelman and C. Mitchell

*Department of Physics, University of California at Los Angeles, 1000 Veteran Avenue, Suite 15-70,  
Los Angeles, California 90095-1696*

(Received 18 December 2001; revised manuscript received 19 June 2002; published 23 January 2003)

Measurements of the dispersion relation for shear Alfvén waves as a function of the perpendicular wave number are reported for the regime in which  $V_A \simeq V_{Te}$ . By measuring the parallel phase velocity of the waves, the measurements can be compared directly to theoretical predictions of the dispersion relation for a parameter regime in which particle kinetic effects become important. The comparison shows that the best agreement between theory and experiment is achieved when a fully complex, warm plasma dispersion relation is used.

DOI: 10.1103/PhysRevLett.90.035004

PACS numbers: 52.35.Bj

Since their prediction by Hannes Alfvén in 1942, Alfvén waves have been found to play a role in a variety of plasmas [1]. In laboratories, they were first observed in the late 1950s [2,3]. Most recently, laboratory experiments have focused on their characteristics for narrow perpendicular scales [4,5]. Shear Alfvén waves are thought to play a significant role in several regions of near-Earth space including the plasma sheet, magnetopause, and auroral zone. For auroral acceleration processes, it is thought that shear mode Alfvén waves are most effective at electron energization when they have narrow perpendicular scale sizes [6–8]. Although the dispersion relation for these waves has been derived by several authors, direct experimental measurements to verify the dispersion relation have been few.

Two limits, corresponding to cold or hot electrons, are typically considered: the inertial ( $V_{Te} \ll V_A$ ) or kinetic ( $V_{Te} \gg V_A$ ) modes of the shear Alfvén wave. The interesting physics occurs when the waves have narrow perpendicular structure, that is,  $k_{\perp} c / \omega_{pe} \sim 1$  for the inertial case and  $k_{\perp} \rho_s \sim 1$  for the kinetic case. When the perpendicular size approaches these scale sizes, the particle kinetic effects become important and modify the wave physics such that the usual MHD description is no longer valid. In this Letter we describe a set of experiments which probe the dispersion relation for the intermediate regime of temperature where  $V_{Te} \simeq V_A$  such that neither the kinetic nor inertial limit applies. This allows us to test theoretical predictions of the dispersion of these waves by direct comparison with data.

The experiments we describe were conducted in the Large Plasma Device (LAPD) at the University of California at Los Angeles which produced a plasma column of 10 m length and 40 cm diameter. The experiments were conducted in a fully ionized helium plasma with density of  $1.6 \times 10^{12} \text{ cm}^{-3}$ . The electron temperature was measured with a swept Langmuir probe and found

to be  $3.05 \pm 0.20 \text{ eV}$  in the region where the waves were launched. No temperature measurements were made of the ions, but they are assumed to have a temperature of 1 eV based on interferometric measurements made under similar plasma conditions. The background magnetic field was set at 700 and 1000 G which yields ratios of electron thermal speed to Alfvén speed of  $V_{Te}/V_A = 1.25$  and  $V_{Te}/V_A = 0.88$ , respectively. For these plasma parameters, the skin depth,  $c/\omega_{pe}$ , is 0.42 cm and the ion acoustic gyroradius (the gyroradius of ions with energy equal to that corresponding to the electron temperature),  $\rho_s$ , is 0.53 cm for 700 G and 0.37 cm for 1000 G. For both cases, the waves were launched by emitting a tone burst of five periods at a frequency just slightly greater than half the ion cyclotron frequency ( $\omega/\omega_{ci} = 0.525$ ).

In order to produce the narrow perpendicular wavelengths of interest, we have developed a new antenna which consists of a series of 14 vertical grid elements of 8.9 cm length on 0.64 cm centers. Each grid can be driven independently to produce a variety of spatial waveforms. In all cases, to produce an Alfvén wave, all 14 grids are biased to a positive voltage to collect electron current along the magnetic field. We refer to this potential as the “float” bias. The electron current is then modulated around this intermediate current level. This is done because the ion saturation current limits the current drawn by the anode for negative voltages to small values, resulting in very small amplitude waves.

For the work reported here, the antenna pattern had the outermost grids at the float potential and the inner grids were driven with the following spatial pattern: positive (in-phase), float, negative (out-of-phase), float, and repeating twice more for the remaining eight grids. This results in a spatial waveform of three complete wavelengths across the antenna. To illustrate this pattern, Fig. 1 shows an example of a single snapshot in time of a plane of magnetic field data (the vertical component)

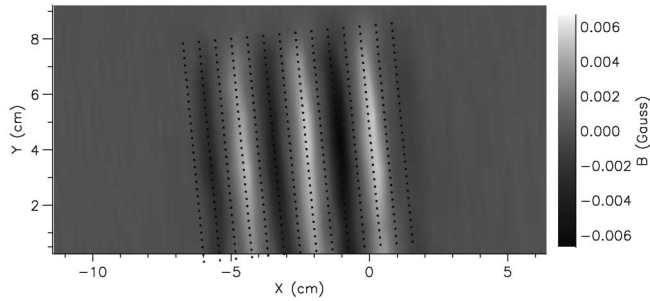


FIG. 1. Example of a plane of magnetic field measurements from the LAPD showing a snapshot in time of a propagating Alfvén wave with narrow perpendicular structure. The dotted lines show the approximate locations of the individual antenna elements which drive the structure. Note that the antenna was slightly rotated from purely vertical by  $\sim 5^\circ$  which has been accounted for in the analysis.

taken at about a meter from the antenna. The dotted lines in the figure outline the approximate locations of the antenna grid elements. The background magnetic field is out of the plane of the figure, and thus the figure represents magnetic field variation perpendicular to the magnetic field and along the vertical axis. Because the antenna also couples to longer wavelengths, the data shown in Fig. 1 have had a large spatial scale average subtracted from them to highlight the narrow structures which the antenna drives.

The magnetic field data were taken using three-axis search coil probes with diameters of 5 mm. Data were sampled on a rectangular grid with horizontal spacing of 1.5 mm and vertical spacing of 1 cm. The higher horizontal sampling was done to get maximum resolution in the direction of greatest variation. In time, each grid location is sampled at 25 Msamples/s. The extremely good repeatability of the LAPD allows us to average 20 shots at each grid point to reduce noise and better resolve the wave signal we wish to measure.

There are two advantages in using this type of antenna system. The first is that it emphasizes discrete wavelengths which are harmonically related to the base pattern (both longer and shorter harmonics are excited). This allows more power to be coupled to the plasma at these harmonics than can be coupled with antennas which excite a broad, relatively continuous range of wave numbers. Model studies of the power spectra generated by our antenna show that the power is increased by a factor which is roughly the number of wavelengths in the pattern. Hence the three wavelength pattern shown in Fig. 1 has 3 times more power at its harmonics than a single antenna element would generate. This is important because it permits measurement of damped wavelengths at higher damping factors than could otherwise be achieved. A second advantage is that the antenna is relatively compact compared with a system such as that used by Ono [9] which set the parallel wavelength instead of the perpendicular wavelength. For Alfvén waves in the LAPD, this would require an arrangement of anodes more than

4 m in length which becomes unwieldy to implement experimentally.

To compare these measurements with the dispersion relation for shear Alfvén waves, the parallel phase velocity of the wave is determined as a function of perpendicular wave number. To do this, a single line of data, taken horizontally across the pattern and near the center vertically, is Fourier transformed in space at each time step to yield the perpendicular wave number spectrum as a function of time. Implicit in this technique is the assumption that we may ignore variation in the vertical direction. As Fig. 1 shows, this is a reasonable assumption due to the lack of variation along the vertical direction near the center of the wave pattern. This procedure is then repeated for a second location farther away from the antenna and the two Fourier-transformed data sets are compared to determine the propagation time between the two locations.

An example of one of these comparisons is shown in Fig. 2. The top panel [2(a)] shows two different time series of a single component of  $k_\perp$  (the same for each time series) taken from the spatial Fourier transform at two different distances from the antenna for the same input signal. The injected signal for this example is a tone burst of five periods at a frequency of 140 kHz. The measurements closest to the antenna are those with the largest amplitude, and the smaller amplitude measurements are those taken farther away.

In Fig. 2(a), both sets of measurements are shown with the same offset in time with respect to the antenna signal; that is, both have the same start time. As can be clearly

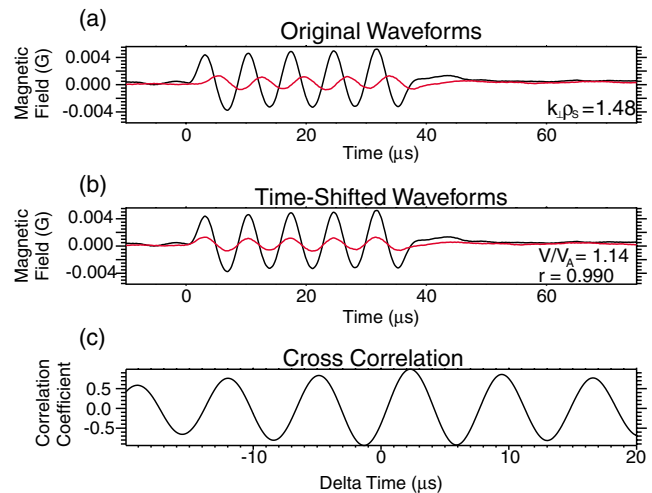


FIG. 2 (color online). Correlation measurements for a single wave number ( $k_\perp \rho_s = 1.48$ ). (a) The original waveforms as measured at two different locations. (b) The waveforms after shifting by the amount of time given by the peak cross correlation. (c) The cross correlation as a function of offset time with a peak at  $2.3 \mu\text{s}$ . By using the distance between the two measurements combined with this time shift, the phase velocity of the wave can be determined.

seen, the smaller amplitude signal arrives later at the plane where it is measured because it is farther away from the antenna. Figure 2(b) shows the result of shifting the smaller signal with respect to the larger signal by a time given by the greatest cross correlation coefficient [shown in Fig. 2(c)] between the two signals. The correlation is the usual linear cross correlation used for statistically relating arrays of numbers [10]. The periodic nature of the waveform causes a pattern similar to interference fringes which decreases in amplitude away from a peak linear correlation value of  $r = 0.990$  at  $2.3 \mu\text{s}$ .

The time delay is combined with the measured distance of 1.55 m between the two sets of measurements to determine a velocity. The correlation technique is optimized to produce the greatest correlation for alignment of the peaks of the two waveforms rather than the envelope of the waveform. This is done to ensure that the velocity which is found corresponds to the parallel phase velocity of the wave  $V_{ph,\parallel} = \omega/k_{\parallel}$ .

By repeating this procedure at each wave number with significant power above the background noise level, a set of measurements of the parallel phase velocity as a function of perpendicular wave number is generated. In all cases, the linear correlation coefficients determined by this procedure exceed  $r = 0.98$ , confirming the assumption that the signal at the two measurement locations is the same wave which has propagated along the magnetic field. Two sets of phase velocity determinations, made from the three wavelength antenna pattern, are shown in Fig. 3. The upper panel shows measurements for which  $V_{Te}/V_A = 1.25$ . The lower panel shows measurements for which  $V_{Te}/V_A = 0.88$ . In both cases all plasma parameters were maintained at essentially the same values except for the background magnetic field which was changed to control the Alfvén speed  $V_A$ . The measurements are shown in normalized coordinates; the perpendicular wave number is normalized to the ion acoustic gyroradius  $\rho_s$ , and the phase velocity is normalized to the Alfvén speed  $V_A$ .

For both cases shown in Fig. 3, the ratio of electron thermal speed to that of the Alfvén speed  $V_{Te}/V_A$  is close to 1. Consequently, neither set of measurements can be considered to be inertial or kinetic and the usual simplification of the dispersion relation that results for those cases does not apply. Instead, we must turn to the warm plasma dispersion relation appropriate for waves with finite frequency with respect to the ion gyrofrequency given by

$$Z'(\zeta) \left\{ \frac{V_A^2}{V_{Te}^2} \left[ \frac{(1 - \frac{\omega^2}{\omega_{ci}^2})\mu}{1 - e^{-\mu} I_0(\mu)} \right] - \zeta^2 \right\} = \frac{k_{\perp}^2 c^2}{\omega_{pe}^2}, \quad (1)$$

where  $\zeta = \omega/k_{\parallel} V_{Te}$ ,  $\mu = k_{\perp}^2 \rho_i^2$ , and  $Z'(\zeta)$  is the derivative of the plasma dispersion function [11,12]. In Fig. 3, the phase velocity as a function of perpendicular wave number as determined by numerically solving (1) has been plotted as a solid line for comparison with the data. Two additional curves are plotted on either side

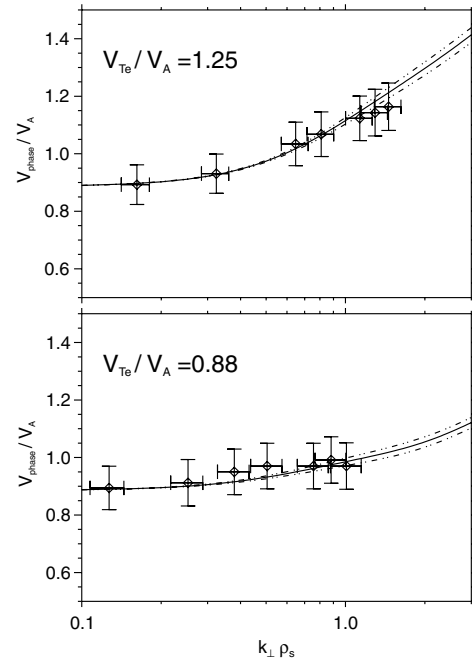


FIG. 3. A comparison of the dispersion relation with the measurements as a function of perpendicular wave number for two cases. For comparison, the theoretical dispersion relation, cast in the form of parallel phase velocity vs  $k_{\perp}\rho_s$ , is plotted as a solid line.

which represent the variation in the analytical result due to varying the electron temperature by 1 standard deviation. For both cases, the agreement between theory and measurement is quite good. This result has been corrected for the slight rotation of the antenna evident in Fig. 1. In solving for the phase velocity, complex frequency has been used which includes a collision operator. The effect of including finite frequency introduces the frequency ratio term in the numerator of the left hand side of Eq. (1). Physically, this lowers the background Alfvén phase velocity. This is seen clearly at small values of  $k_{\perp}\rho_s$  in both panels of Fig. 3 where the normalized phase velocity is less than one.

It is important to include the effects of damping in this regime because the electron thermal speed is very close to the wave phase velocity allowing significant transfer of energy to the electrons. Indeed, without including the imaginary parts of  $\omega$ , no roots for (1) can be found. The effect of damping is seen in the waveforms in Fig. 2; the wave measured farthest from the antenna has distinctly smaller amplitude. This is shown more clearly in Fig. 4 which shows measured and theoretical damping as a function of  $k_{\perp}\rho_s$ . The experimental values are determined by using the amplitude decrease between locations and the propagation time to compute a damping rate which is normalized to the wave frequency. The theoretical damping includes a nonconserving Krook collision term as well as Landau damping. The measured damping agrees with theoretical damping at small values of  $k_{\perp}\rho_s$ . For values of  $k_{\perp}\rho_s > 1$ , the agreement is not as good,

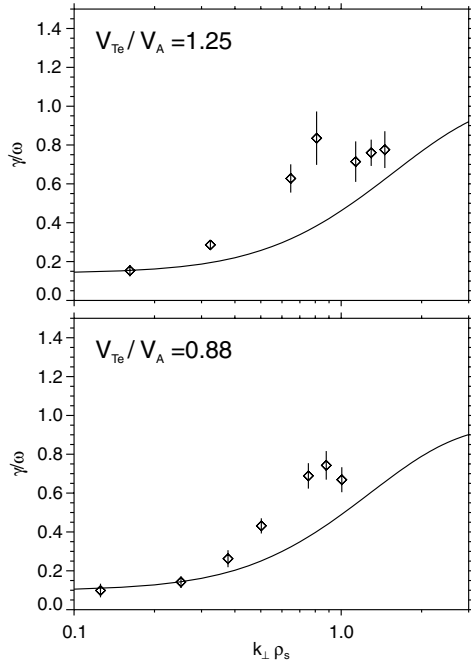


FIG. 4. A comparison of the measured damping rate with the measurements as a function of perpendicular wave number for two cases. The theoretical damping is plotted as a solid line.

with an approximately 30% mismatch, but the basic trend is correct. However, we do find significant disagreement for normalized wave numbers just below  $k_{\perp}\rho_s = 1$ . Note that this occurs for both sets of measurements for the same range of wave numbers. The enhanced damping just below  $k_{\perp}\rho_s = 1$  is not yet understood. One possibility is that this may be a coupling to drift waves which anomalously damp the waves. Work is currently underway to investigate the enhanced damping for these wave numbers and will be reported in a future communication. The damping plays a role in the real part of the dispersion relation, but the disagreement shown does not affect the theoretical curves in Fig. 3 enough to move them outside the error bars and therefore does not change the basic result.

Although (1) gives the precise dispersion relation for comparison with the measurements, it does not provide the most intuitive form for understanding the physics. For this we turn to fluid theory, for which the dispersion relation for nonideal, shear Alfvén waves with finite ion temperature [12] is

$$\frac{\omega}{k_{\parallel}} = V_A \sqrt{\frac{1 + k_{\perp}^2 \rho_s^2 (1 + T_i/T_e)}{1 + k_{\perp}^2 c^2 / \omega_{pe}^2}}. \quad (2)$$

In this form, it can be seen that the parallel phase velocity is solely a function of  $k_{\perp}$ ; measurement of the parallel phase velocity directly verifies the dispersion relation (2). For the case at hand, in which we have finite frequency with respect to the cyclotron frequency, the phase speed will not be appropriately reduced; only the kinetic ap-

proach described above can properly include this effect. Lysak and Lotko [13] have shown that (2) is often a very good approximation to the full kinetic dispersion relation in the low frequency limit.

Except for the overall lowering of the phase velocity due to the finite frequency correction, the fluid dispersion relation illustrates the competition between ion and electron kinetic effects. For the measurements shown in the upper panel of Fig. 3, the  $c/\omega_{pe}$  is about 20% smaller than  $\rho_s$ , and hence the phase speed will grow as the perpendicular length scale approaches the ion acoustic gyroradius. However, because  $c/\omega_{pe}$  is also close to  $\rho_s$ , the phase speed does not grow as fast as would be expected for the purely kinetic limit of the dispersion relation in which the denominator is set to unity. This effect is even clearer in the lower panel of Fig. 3 because these two length scales are very close to identical and, consequently, the phase speed rises even more slowly as a function of increasing  $k_{\perp}\rho_s$ .

We have made what we believe are the first detailed measurements of the phase velocity of shear Alfvén waves for the case which is intermediate between the inertial and kinetic limits. The agreement between the complex, warm plasma dispersion relation result and experiment is good, showing that the dispersion relation for shear Alfvén waves holds for this intermediate regime. In this regime, a simple fluid picture gives the basic physics of the two competing limits, but is inadequate to handle the finite frequency correction and damping effect which require that kinetic effects be included.

Funding was provided by NSF Grant No. ATM-9806868. The authors thank A. Bhattacharjee, P. Zhu, D. Leneman, and S. Vincena for helpful discussions.

\*Electronic address: craig-kletzing@uiowa.edu

- [1] H. Alfvén, *Nature (London)* **150**, 405 (1942).
- [2] T. K. Allen, W. R. Baker, R. V. Pyle, and J. M. Wilcox, *Phys. Rev. Lett.* **2**, 383 (1959).
- [3] D. F. Jephcott, *Nature (London)* **183**, 1652 (1959).
- [4] W. Gekelman, D. Leneman, J. Maggs, and S. Vincena, *Phys. Plasmas* **1**, 3775 (1994).
- [5] W. Gekelman, S. Vincena, D. Leneman, and J. Maggs, *J. Geophys. Res.* **102**, 7225 (1997).
- [6] A. Hasegawa, *J. Geophys. Res.* **81**, 5083 (1976).
- [7] C. A. Kletzing and S. Hu, *Geophys. Res. Lett.* **28**, 693 (2001).
- [8] R. L. Lysak and C. T. Dum, *J. Geophys. Res.* **88**, 365 (1983).
- [9] M. Ono, *Phys. Rev. Lett.* **42**, 1267 (1979).
- [10] W. H. Press, S. A. Teukolsky, W. T. Vetterling, and B. P. Flannery, *Numerical Recipes* (Cambridge University Press, New York, 1992), 2nd ed.
- [11] B. D. Fried and S. D. Conte, *The Plasma Dispersion Function* (Academic, San Diego, CA, 1961).
- [12] K. Stasiewicz *et al.*, *Space Sci. Rev.* **92**, 423 (2000).
- [13] R. L. Lysak and W. Lotko, *J. Geophys. Res.* **101**, 5085 (1996).